

A New Strategy of Magnetic Design for DC Power Optimizers in Photovoltaic Applications

Dong-Thanh Vu^{1,2,*}, Quoc-Khanh Ngo¹, Quang Bui-Dang¹ and Duy-Dinh Nguyen¹

¹ Hanoi University of Science and Technology, Hanoi, Vietnam

² EVSELab Co., Ltd., Vietnam

*Corresponding author E-mail: vudongthanh04210@gmail.com

Abstract

This research introduces a novel approach to selecting and designing magnetic cores for DC power optimizers. Unlike traditional methods that depend on the Area Product (A_p) and involve extensive trial and error to achieve the final design, the proposed methodology utilizes two essential parameters: the Core to Copper Loss Ratio (γ) and the Window Utilization Factor (k_w) for the inductor design process. The loss models of the inductor are formulated based on these variables, considering the impact of DC bias, a crucial factor that significantly affects the inductor in high magnetic field strength applications. To minimize the overall magnetic loss, the PSO algorithm is applied. The simulation results validate the effectiveness and rationality of the proposed magnetic models and optimization strategy. Therefore, this approach provides an efficient and effective alternative to the traditional trial-and-error approach for designing and selecting magnetic cores for DC power optimizers.

Keywords: Magnetic design, Inductor design, DC optimizer, Optimization algorithm.

1. Introduction

In recent years, there has been an increasing interest in photovoltaic (PV) energy as a potential alternative energy source that can reduce carbon emissions and provide a sustainable energy supply [1]. The conversion of PV power to the grid requires the use of a power converter to optimize energy efficiency and ensure that the output voltage and current meet grid requirements [2]. One of the most commonly used power converters in PV applications is the boost converter topology [3]. This DC-DC converter can increase the voltage of a DC input to a higher level, making it useful in PV applications where it can increase the low DC voltage output of a solar panel to a level suitable for feeding into the grid [2]. By applying maximum power point tracking algorithms (MPPT), the boost converter can also transfer maximum energy from the PV module to the inverter stage, making it a DC optimizer or DC power optimizer.

Designing a DC optimizer for a PV system poses several challenges due to the unique characteristics of the PV source and the grid connection requirements, such as variable and unpredictable input voltage, MPPT algorithms, thermal management, and magnetics design, among others, [2], [4]. The magnetic design of the DC optimizer is critical to its optimal performance. The design of magnetic components, such as the inductor and transformer, determines the efficiency and reliability of the converter [4]. Proper magnetic design can lead to higher efficiency, lower power losses, and reduced component size and

weight. However, the magnetic design process is complex and requires an understanding of various parameters and trade-offs. Several magnetics design methodologies have been published in the literature, providing design guidelines for creating magnetic components based on fundamental concepts [5–7]. Typically, these guidelines suggest a step-by-step process that includes core selection, conductor selection, loss evaluation, and other parameter estimation. However, the core selection is typically based only on an appropriate Area-Product (A_p) parameter, which is independent of the converter's performance. Therefore, it requires repeating the process multiple times to achieve an optimal design. In [8], the author used observation and approximation methods to show the relationship between A_p and the total loss of magnetic components. However, the process still involves trial and error to obtain good results. To address this issue, report [9] used the 3D-graphical method for surveying and selecting a suitable design. However, these methods have not considered the effect of DC bias, which can significantly affect the final design. In PV applications, the boost converter operates with low voltage and high current, making this impact more significant.

This paper proposes a new approach to inductor design for a DC power optimizer. The winding loss (P_{cu}) and ferrite loss (P_{fe}) are formulated in terms of A_p . To enhance accuracy, the effect of DC bias is also addressed in modeling the inductor loss. The PSO algorithm is employed to find the optimal design. Inequality constraints were considered in the optimization

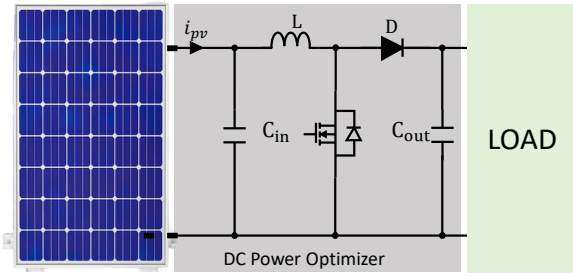


Figure 1: DC Power Optimizer

problem due to factors such as the limited window area of the inductor and the need to handle the operating temperature. The optimized inductor was then verified by finite element method magnetic (FEMM) analysis. Simulation results demonstrate that the loss models of the inductor are reliable.

2. Magnetic Circuit Analysis

2.1. Inductance Analysis

Fig. 1 showed the boost converter topology in PV application, the inductor of which is used to illustrate the design process. The inductance value can be calculated by the following equation (1) [3]:

$$L_0 = \frac{V_{mpp} \cdot D}{f_{sw} \Delta I} \quad (1)$$

where V_{mpp} is the input voltage of the PV,

D is duty cycle,

ΔI is the current ripple of the inductor,

f_{sw} is the switching frequency.

While the inductance value is typically treated as constant throughout circuit operation in designs [5–9], this assumption is not entirely accurate due to the presence of DC bias effect. This phenomenon has a significant impact on inductance value, causing a shift in its frequency response and increasing core losses [10]. This effect causes a mismatch between the designed and actual performance of the inductor, leading to degraded overall system performance. This effect is even more significant in applications with high DC current such as DC power optimizers.

Figure 2 provides an example illustrating how the permeability and the inductance value decrease due to the occurrence of DC bias. It is evident that the inductance value significantly decreases under DC bias, hence in this paper, the inductance value is recalculated based on the operating point of the circuit as the following equation (2):

$$L_b = L_0 \cdot k_b \quad (2)$$

where L_b is recalculated inductance value; k_b is the DC bias gain which depends on the magnetic core material. In this paper, the magnetic core of Micrometal manufacture is used to illustrate the design process. From [11], k_b can be expressed

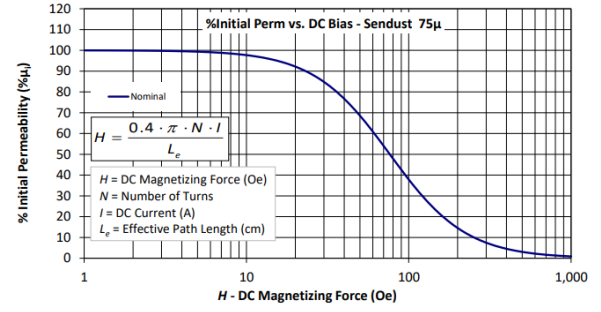


Figure 2: Percent of permeability vs DC Bias [11]

by the Equation (3):

$$k_b = \frac{1}{\frac{1}{a_1 + b_1 B_{ac}^{c_1}} + \frac{1}{d_1 B_{ac}^e} + \frac{1}{f_{sw}}} \quad (3)$$

where a_1, b_1, c_1, d_1 and e is the material coefficients; B_{ac} is AC flux density of magnetic core.

2.2. Core Parameters Formulation

The design of an inductor typically begins with selecting a core [5–7]. An initial core selection is based on the core area product (A_p) which is the product of W_a and A_c . The A_c and W_a of the magnetic core are illustrated in Fig.3. The product of them specifies the energy handling capability of the core and is defined by equation (4):

$$A_p = W_a \times A_c = \frac{2(\text{Energy})(10^4)}{B_m J k_u} \quad (4)$$

where B_m is the maximum flux density; J is current density; k_u is window utilization factor.

In [5–7], by selecting B_m, J and k_u , the initial parameters of A_p can be determined. Subsequently, the number of turns and type of wire is calculated based on the design inductance value, followed by the assessment of losses and temperature rise. However, this process does not take into account the impact of DC bias as analyzed in Section 2.1. Additionally, numerous trial and error iterations are typically required to arrive at the final design, while ensuring that parameters such as losses and temperature rise meet the specified requirements.

To streamline the design process, this paper proposes a loss model that accounts for the effect of DC bias and applies an optimization algorithm to find out the inductor which has the lowest loss. Computed-aided tools are employed to support the design process, thereby reducing the workload of the designer and resulting in a more accurate design.

The first step in this design process is to reformulate A_p related to magnetic mechanical, electromagnetic, and power dissipation parameters. This relationship is described in [8] as following equation (5):

$$A_p = \left[\frac{\sqrt{1 + \gamma K_i L_b I_{\max}}}{B_m K_t \sqrt{k_u \Delta T}} \right]^{\frac{8}{7}} \quad (5)$$

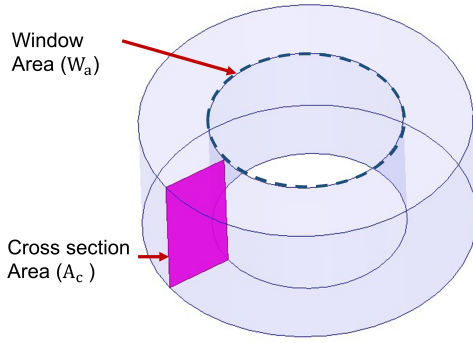


Figure 3: Magnetic core illustration.

where $\gamma = P_{fe}/P_{cu}$ is core to copper loss ratio,

K_i is root-mean-square to maximum inductor current ratio,

L_b is the inductance value calculated in 2,

K_t is a dimensional constant,

ΔT is the temperature rise of the inductor.

The key characteristics and physical measurements of the core, including W_a , A_c , core volume (V_c), the mean length turn (MLT), the magnetic path length of the core (l_e), winding volume (V_w) and total surface area (A_t), can be determined based on the value of A_p using dimensional analysis, as explained in the references [8, 12]. In order to simplify the number of unknown factors, [9] introduced a ratio of W_a to A_c , which can be expressed by the following equation (6):

$$x = \frac{W_a}{A_c} \quad (6)$$

Therefore, the values of W_a , A_c , V_c , and l_e that correspond to each A_p value can be calculated by using the equations described in (7):

$$\begin{cases} W_a = \sqrt{A_p \times x} \\ A_c = \sqrt{\frac{A_p}{x}} \\ V_c = k_c \times A_p^{\frac{3}{4}} \\ l_e = \frac{V_c}{A_c} \end{cases} \quad (7)$$

where k_c depends on geometry and the manufacture; $k_c = 5.6$ with vertical core and $k = 3.3$ with toroidal core typically [8]. Then the current density (J) within the winding needs to meet the maximum allowable temperature and can be expressed in terms of k_u , γ , ΔT and A_p as the following equation (8):

$$J = K_t \frac{\sqrt{\Delta T}}{\sqrt{k_u(1+\gamma)} \sqrt[3]{A_p}} \quad (8)$$

Next, it is possible to calculate the inductance value in terms of the number of turns (N) and core reluctance (\mathfrak{R}):

$$L = \frac{N^2}{\mathfrak{R}_{\text{core}}} \quad (9)$$

where N and R_e can be calculated by (10) and (11):

$$N = \frac{k_u W_a}{A_w} \quad (10)$$

$$R_e = \frac{l_e}{\mu \mu_r A_c} \quad (11)$$

2.3. Loss Formulation

Inductor loss includes ferrite loss on the magnetic core and copper loss dissipating on windings as follows by equation (12):

$$\Delta P_{ind} = P_{fe} + P_{cu} \quad (12)$$

From [11] the core loss can be estimated by the following equation (13):

$$P_{fe} = V_c \cdot \left(\frac{f_{sw}}{\frac{a_2}{B_{ac}^3} + \frac{b_2}{B_{ac}^{2.3}} + \frac{c_2}{B_{ac}^{1.65}}} + d_2 \cdot B_{ac}^2 \cdot f_{sw}^2 \right) \quad (13)$$

where a_2, b_2, c_2, d_2 is core loss coefficients

Substituting (7) to (13), P_{fe} can be calculated in terms of A_p , by following equation (14):

$$P_{fe} = k_c \times A_p^{\frac{3}{4}} \cdot \left(\frac{f_{sw}}{\frac{a_2}{B_{ac}^3} + \frac{b_2}{B_{ac}^{2.3}} + \frac{c_2}{B_{ac}^{1.65}}} + d_2 \cdot B_{ac}^2 \cdot f_{sw}^2 \right) \quad (14)$$

The basic formula of the copper loss can be expressed as the following equation (15):

$$P_{cu} = R_{dc} I_{rms}^2 \quad (15)$$

Apply approximation methods, [9] reports a calculation of the copper loss in terms of A_p , k_u and J as following equation (16):

$$P_{cu} = k_w \cdot A_p^{\frac{3}{4}} \times \rho_w \times k_u \times J^2 \quad (16)$$

where ρ_w is the resistivity of copper winding; $\rho_w = 1.68 \times 10^{-8}$, k_w depends on types of cores, $k_w = 8$ with toroidal core.

3. Design Method

3.1. Design Constraints

The overall power dissipation of the inductor should be minimized in order to maximize system efficiency. The inductor is dropped by the DC bias as described in Section 2 for a given input parameters ($V_{mpp}, P_{rate}, B_m, \Delta T$), the tuning parameters are γ , k_u and x . Then, some additional constraints are applied to optimize the design.

The first physical constraint is to limit the winding current density in order to prevent overheating and damage to the material or conductor. High current densities can result in an increase in temperature, which can lead to thermal expansion, changes in material properties, and even melting or breakdown of the material [13], as shown in (17):

$$J_{min} < J < J_{max} \quad (17)$$

Next the inductance value (L) in (9) needs to be limited to obtain the design requirement given by (18):

$$L \leq L_0 \pm 5\% \quad (18)$$

Then the inductance value at peak current should not decrease more than 30% from the initial value, this inductance value is limited by (19):

$$L_b \geq 70\% \times L \quad (19)$$

The window utilization factor (k_u) needs to be limited to avoid magnetic saturation of the core, which can result in increasing loss of the inductor and an increase in winding resistance, leading to decreased efficiency and potential damage to the inductor [6], which should be restricted by (20):

$$k_{u_{min}} \leq k_u \leq k_{u_{max}} \quad (20)$$

The ratio of core loss to copper loss (γ) in an inductor is an important consideration for the efficient design of the inductor. The range of this ratio needs to be limited by (21):

$$\gamma_{min} \leq \gamma \leq \gamma_{max} \quad (21)$$

Finally, the range of W_a to A_c ratio (x) is also considered because of the core geometry reality. By comparing several core options, it was found that this ratio typically varies between 2 and 6 [9] and is shown in (22):

$$x_{min} \leq x \leq x_{max} \quad (22)$$

3.2. Objective Function

The primary purpose of this study is to design a lowest-loss inductor. Therefore, the objective function is to minimize the inductor loss. The equation (23) derives the objective function equation from this study:

$$f(\gamma, k_u, x) = \Delta P_{ind} \rightarrow \min \quad (23)$$

Minimization of f must meet the predetermined constraints as described in Section 3.1. Equations (24) contain constraints that must be appropriate in this inductor design:

$$\begin{cases} c_1(\gamma, k_u, x) = J - J_{max} \leq 0 \\ c_2(\gamma, k_u, x) = J_{min} - J \leq 0 \\ c_3(\gamma, k_u, x) = L - L_0 \cdot (1 + 5\%) \leq 0 \\ c_4(\gamma, k_u, x) = L_0 \cdot (1 - 5\%) - L \leq 0 \\ c_5(\gamma, k_u, x) = 70\% \times L - L_b \leq 0 \\ c_6(\gamma, k_u, x) = k_u - k_{u_{max}} \leq 0 \\ c_7(\gamma, k_u, x) = k_{u_{min}} - k_u \leq 0 \\ c_8(\gamma, k_u, x) = \gamma_{min} - \gamma \leq 0 \\ c_9(\gamma, k_u, x) = \gamma - \gamma_{max} \leq 0 \\ c_{10}(\gamma, k_u, x) = x_{u_{min}} - x \leq 0 \\ c_{11}(\gamma, k_u, x) = x - x_{max} \leq 0 \end{cases} \quad (24)$$

Table 1 is a type of optimized design variables along with its lower and upper bounds.

There are numerous methods that can be employed to address the optimization challenges highlighted earlier. However, it is important to note that the optimization function in question involves a round-up or ceiling function, which renders it discontinuous and non-differentiable at that point. As a result, the use of explicit gradient-based techniques is not viable, and alternative approaches are required. One such alternative approach is

Table 1: Lower and upper bounds for genetic algorithm

Parameter	Symbol	Lower Bound	Upper Bound
Current density	J	1 A/mm ²	9 A/mm ²
Window utilization factor	k_u	0.05	1
Core to copper loss ratio	γ	0.5	5
W_a to A_c ratio	x	2	6

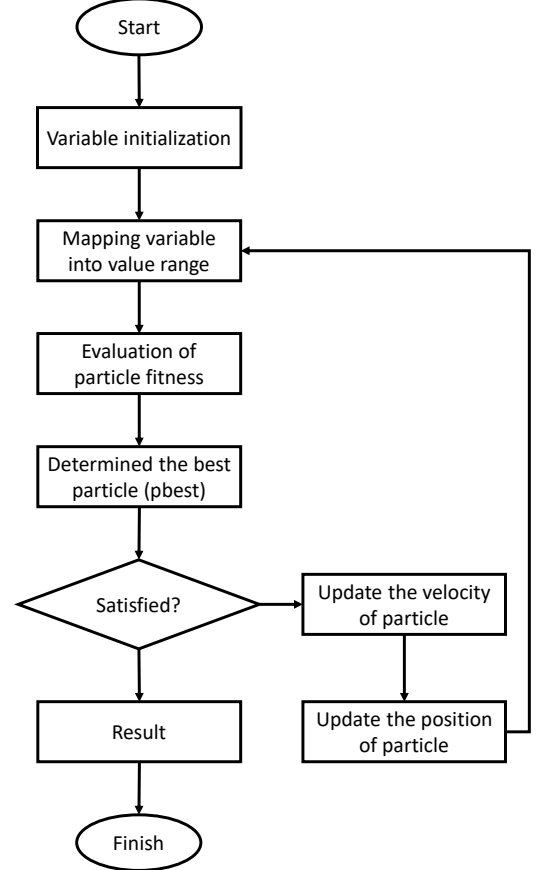


Figure 4: The flowchart of the PSO model

the use of heuristic techniques like the genetic algorithm (GA), differential evolution (DE), and particle swarm optimization (PSO), among others, as they can effectively tackle problems that are not amenable to gradient-based techniques [14]. In this particular study, the PSO approach was adopted due to its simplicity, ease of implementation, and feasibility for the problem at hand.

3.3. Principle of Particle Swarm Optimization

PSO is an optimization search algorithm based on swarm behavior. PSO is an algorithm based on population, exploiting the population to find potential solutions in the search space. The population is called a swarm, and the individual is called a particle [15].

$$S = \{x_1, x_2, x_3, \dots, x_N\} \quad (25)$$

$$x_i = (x_{i1}, x_{i2}, x_{i3}, \dots, x_{iN})^T \in A \quad (26)$$

The objective function is assumed to be available for all points in space A, and the particles move in search space A with ve-

Table 2: The PSO parameters.

Parameter	Value
Number of particles	250
Number of optimized variables	3
Number of the maximum iteration	30
Cognitive parameter	3
Social parameter	3

Table 3: Specification parameters

Parameter	Symbol	Value	Unit
Rated Power	P_{rate}	550	W
MPP Voltage	V_{mpp}	45	V
Switching Frequency	f_{sw}	30	kHz
Inductance Value	L	120	μH
Peak Flux Density	B_m	500	mT
Temperature rise	ΔT	40	$^{\circ}\text{C}$

locity v_i . The velocity and position of each particle are updated interactively to allow the particle to find any point in space A.

$$v_i = (v_{i1}, v_{i2}, v_{i3}, \dots, v_{iN})^T \quad i = 1, 2, \dots, N \quad (27)$$

The equations provided in (28) and (29) are the velocity and position update equations for each particle. The velocity update equation in (28) takes into account the best position (p_{ij}) the particle has ever obtained and the particle's current position (x_{ij}). The cognitive parameter (c_1) and social parameter (c_2) weigh the influence of the particle's current position and the best position the particle has ever obtained, respectively. The random variables R_1 and R_2 add stochasticity to the velocity update equation (28):

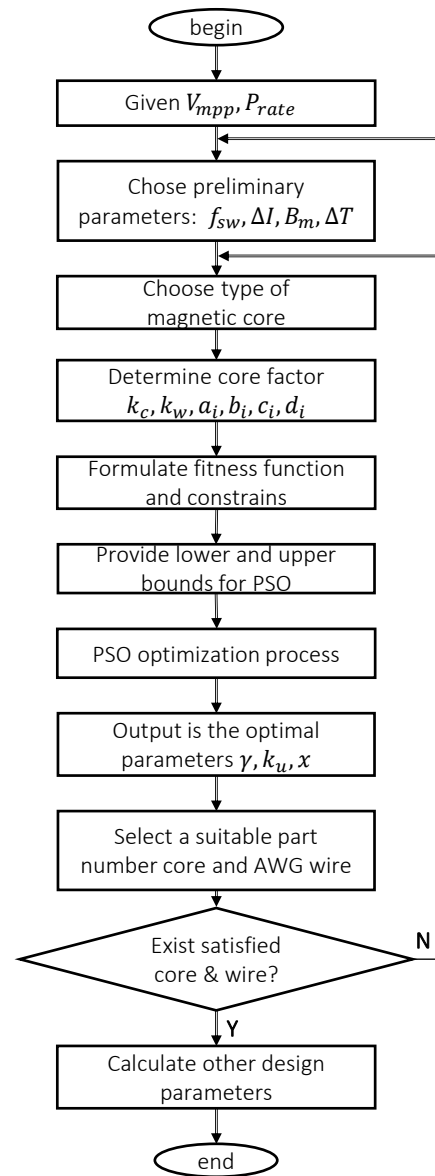
$$v_{ij}(t+1) = v_{ij}(t) + c_1 R_1 (p_{ij}(t) - x_{ij}(t)) + c_2 R_2 (p_{ij}(t) - x_{ij}(t)) \quad (28)$$

$$x_{ij}(t+1) = x_{ij}(t) + v_{ij}(t+1) \quad (29)$$

After updating and evaluating the particles in each iteration, the best position of the particles will be updated. This algorithm has advantages such as a simple program, high-quality solution, and fast convergence [15]. Figure 4 helps to visualize the flow of the PSO algorithm.

3.4. Case Study

This design is applied to the boost DC optimizer circuit, with the specifications shown in Table 3. The constraints are used based on Equation (24), and the lower bounds and upper bounds of each optimized design variables are presented in Table 1. In contrast, the PSO parameters are shown in Table 2. The flowchart of the entire design process is described in Fig.5. The design problem is initiated by specifying the rated power (P_{rate}) and input voltage of the converter (V_{mpp}). Subsequently, preliminary parameters such as the switching frequency, the maximum flux density, the desired temperature, and the inductance value are pre-selected. From the design's core type and material, the core's characteristic parameters are extracted to establish the loss model for the inductor. The constraints of parameters are provided to ensure the design's feasibility

**Figure 5:** Design Process

and practicality. The loss model and the parameter constraints are the inputs into the PSO algorithm to obtain the value of γ , k_u and x . The satisfied core size and winding wire are then derived from these values. The design process terminates when the combination of a core and winding wire that satisfies the design output is identified. Otherwise, the preliminary parameters or core type need to be re-evaluated and modified. This iterative process continues until the final outcome is the inductor with the lowest total loss.

4. Results, Comparison and Discussion

4.1. Optimization Result

The results of the design process are displayed in Fig.6. The x-axis of Fig.6a represents the number of iterations that the PSO algorithm has run for, while the y-axis of this figure 6a represents the fitness of the best individual in the population at each iteration. The fitness of the best individual in the population generally improves over time as the PSO algorithm runs

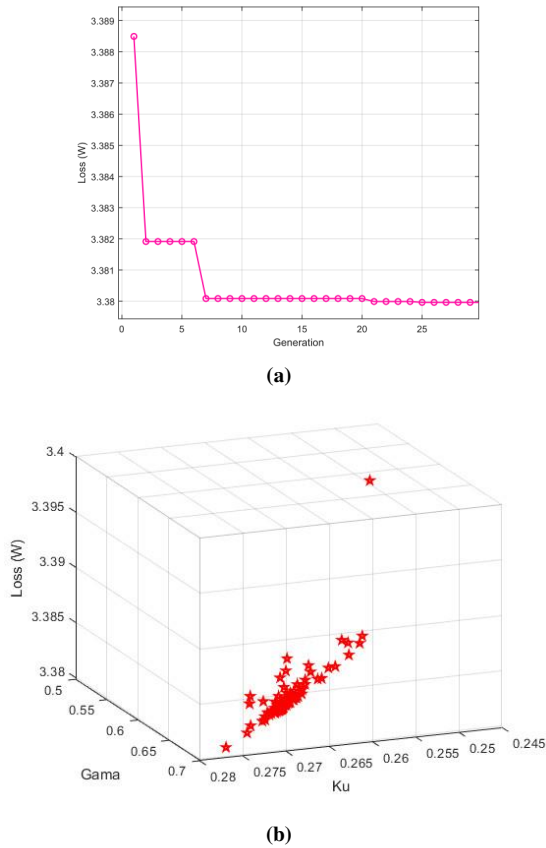


Figure 6: PSO Algorithm Results:

(a) The objective function value (b) Optimization of positioning

Table 4: Calculated core parameters

Parameter	Symbol	Calculation	Unit
Core to copper loss ratio	γ	0.537	
Window utilizing factor	k_u	0.251	
W_a to A_c ratio	x	4.01	
Window area product	A_p	4.263	cm ⁴
Inductance at initial	L_0	127.94	μ H
Inductance at peak current	L_b	90.15	μ H
Number of turns	N	35	turns
Total loss	P_{tot}	3.380	W
Core loss	P_{fe}	1.202	W
Copper loss	P_{cu}	2.178	W

and converges after about 30 iterations. These properties are illustrated in Fig.6b which shows the 3D plot of the total loss and the variables of a fitness function. It can be observed that the cost of individuals in the 30th iteration is going forward nearly on the point of the global best, which means the PSO algorithm has found the optimal point.

The optimal fitness value, which corresponds to the minimum inductor loss, is achieved at 3.380 W for a particular set of parameters (γ, k_u, x) with values of (0.537, 0.251, 4.01). Table 4 shows other important parameters. The core MS-157075-2 of Micrometal manufacture and AWG 12 wire are selected to match the above parameters.

4.2. Comparison

The comparison of proposed results is necessary to indicate the differences between the conventional A_p method and the given optimal method. The A_p method is illustrated clearly in

Chapter 9 in [6] with some suggesting parameters; typically, the current density, the flux density, and the temperature rise are selected by 400 A/cm², 0.5 T, and 40 °C, respectively. Hence, the selection of core and wire is conducted through the A_p value and A_w value. After calculating the A_p value of approximately 3.2 and the A_w value of roughly 0.03, the core MS-134075-2 and the AWG 13 are determined. Consequently, the comparison is indicated in the table 5 and Fig.7. The results show total loss of the traditional A_p method is more than the optimal method by approximately 11.9 %, which proves the efficiency of the given approach.

Table 5: Comparison of the given method and the proposed method.

Parameter	The conventional method	The given method
Inductance at initial current	124.97 μ H	127.94 μ H
Inductance at peak current	76.96 μ H	90.15 μ H
Total loss	3.782 W	3.38 W

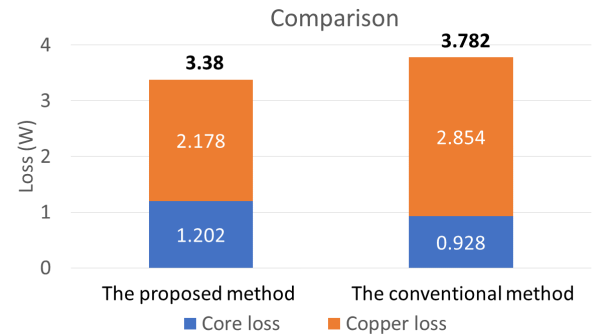


Figure 7: The losses of proposed method and conventional method

4.3. Simulation Results

To validate the designed inductors, a finite-element analysis (FEA) was conducted using the ANSYS Maxwell version 18.0. The FEA results indicated that the flux density within the inductors exhibited a higher density towards the inner edge of the core, while the outer edge had a lower density, as depicted in Fig. 8. This phenomenon can be attributed to the flux seeking the shortest path to flow. The peak flux density was observed to be 562 mT, which satisfied the saturation condition. However, this value exceeded the designed value of 500 mT by 12%. This can be explained by the non-uniform distribution of flux within the magnetic core. While the design value assumes a uniform flux distribution throughout the magnetic core, it is evident that the inside of the inductor has a higher flux density, whereas the edge of the core has a lower flux density than the design value.

Table 6: Calculation and simulation parameters

Parameter	Symbol	Calculation	Simulation
Inductance at initial	L_0	127.94 μ H	128.32 μ H
Inductance at peak current	L_b	90.15 μ H	93.20 μ H
Core loss	P_{fe}	1.202 W	1.26 W
Copper loss	P_{cu}	2.178 W	2.19 W
Peak flux density	B_m	500 mT	562 mT

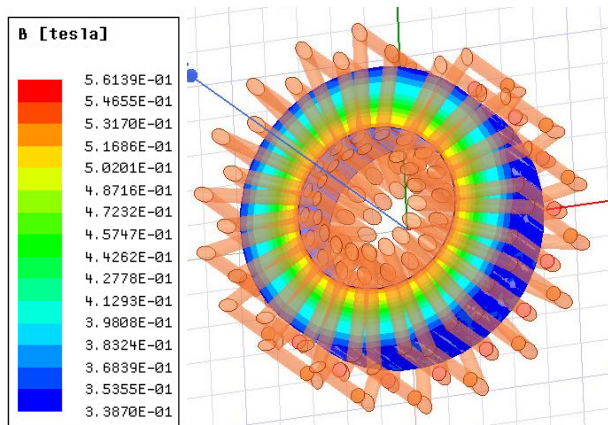


Figure 8: Simulation results with ANSYS Maxwell

Other key parameters, such as the inductance, copper and ferrite losses, were found to be almost identical to the designed values. The comparison between the calculated and simulated values is shown in Table 6. As demonstrated in this table, the calculation parameters matched FEA results very well, with the simulated inductance value of 127.94 μH differing only 0.3% from the expected value of 128.32 μH . Moreover, the inductance value at peak current was observed to decrease to 72.6%, satisfying the DC bias constraint specified in Section 3.1. The prediction of inductor loss was also found to be close to the FEA simulation results. Thus, based on these outcomes, it can be confirmed that the magnetic models and optimization strategy presented in the previous sections are reasonable.

5. Conclusion

This study proposes a novel methodology for designing and selecting magnetic cores for DC power optimizers, which diverges from the traditional approach that relies on the Area Product (A_p) and requires multiple trial-and-error attempts to arrive at the final design. The proposed approach employs two critical starting parameters, namely the Core to DC Copper Loss Ratio (γ) and the Window Utilization Factor (k_u), for the inductor design process. Furthermore, to account for the significant impact of DC bias on the inductor in high magnetic field strength applications, the inductor's loss model are formulated using these variables. The PSO algorithm is utilized to minimize the overall magnetic loss. The simulation results validate that the magnetic models and optimization strategy presented in this study are rational and highly effective. Therefore, this methodology offers a more efficient and effective approach for designing and selecting magnetic cores for DC power optimizers than the traditional trial-and-error approach.

Acknowledgement

This research is funded by Hanoi University of Science and Technology (HUST) under project numbered T2021-SAHEP-005.

References

- [1] J. Yu, Y. M. Tang, K. Y. Chau, R. Nazar, S. Ali, and W. Iqbal, "Role of solar-based renewable energy in mitigating co2 emissions: evidence

- from quantile-on-quantile estimation," *Renewable Energy*, vol. 182, pp. 216–226, 2022.
- [2] F. Belhachat and C. Larbes, "Comprehensive review on global maximum power point tracking techniques for pv systems subjected to partial shading conditions," *Solar Energy*, vol. 183, pp. 476–500, 2019.
- [3] R. Ayop and C. W. Tan, "Design of boost converter based on maximum power point resistance for photovoltaic applications," *Solar Energy*, vol. 160, pp. 322–335, 2018.
- [4] T. Esum and P. L. Chapman, "Comparison of photovoltaic array maximum power point tracking techniques," *IEEE Transactions on energy conversion*, vol. 22, no. 2, pp. 439–449, 2007.
- [5] C. W. T. McLyman, *Magnetic Core Selection for Transformers and Inductors: A User's Guide to Practice and Specifications*. CRC Press, 2018.
- [6] McLyman, *Transformer and inductor design handbook*. CRC press, 2004.
- [7] R. W. Erickson and D. Maksimovic, *Fundamentals of power electronics*. Springer Science & Business Media, 2007.
- [8] W. G. Hurley and W. H. Wölfle, *Transformers and inductors for power electronics: theory, design and applications*. John Wiley & Sons, 2013.
- [9] S. Janghorban, D. G. Holmes, B. P. McGrath, W. G. Hurley, and X. Yu, "Selecting magnetic cores for higher power inductors," in *2016 IEEE 7th International Symposium on Power Electronics for Distributed Generation Systems (PEDG)*. IEEE, 2016, pp. 1–6.
- [10] J. Muhlethaler, J. Biela, J. W. Kolar, and A. Ecklebe, "Core losses under the dc bias condition based on steinmetz parameters," *IEEE Transactions on Power Electronics*, vol. 27, no. 2, pp. 953–963, 2011.
- [11] *Iron Powder Products Catalog*, Micrometal, 2022. [Online]. Available: <https://www.micrometals.com/design-and-applications/literature>
- [12] W. G. Hurley, W. H. Wolfle, and J. G. Breslin, "Optimized transformer design: Inclusive of high-frequency effects," *IEEE transactions on power electronics*, vol. 13, no. 4, pp. 651–659, 1998.
- [13] J. Liu, Y. Wang, C. Wan, S. Lu, and Y.-X. Yin, "Effects of electrolytic copper foil roughness on lithium-ion battery performance," *Journal of The Electrochemical Society*, vol. 159, no. 10, pp. A1671–A1676, 2022.
- [14] V. Kachitvichyanukul, "Comparison of three evolutionary algorithms: Ga, pso, and de," *Industrial Engineering and Management Systems*, vol. 11, no. 3, pp. 215–223, 2012.
- [15] K. E. Parsopoulos and M. N. Vrahatis, "Particle swarm optimization and intelligence: advances and applications: advances and applications," 2010.